混合自适应 RSM-GA 蒙特卡罗优化方法（HRG-MCO）及其在基于加速器的热中子照相慢化体-准直器设计中的应用

Authors: Yang, Mr. Chenxiao, Chen, Dr. Size, Zhang, Dr. Lianxin, Peng, Chuan, Xiao, Mr. Dan, Chen, Dr. Size

Date: 2025-06-04T23:29:16+00:00

Abstract

A new Monte Carlo optimization (MCO) method named Hybrid Adaptive Response Surface Methodology Genetic Algorithm (RSM-GA) Monte Carlo Optimization (HRG-MCO) is proposed to address the strong empirical dependence and low efficiency of global multi-parameter optimization in traditional neutronics design. HRG-MCO integrates the advantages of Response Surface Methodology (RSM) and Genetic Algorithm (GA). Specifically, neutron MC simulation results are iteratively utilized to adaptively construct an RSM model, ensuring the required accuracy. Subsequently, GA is employed to perform multi-parameter optimization based on the constructed RSM model, which makes it possible to rapidly determine the optimal design parameters. Then, these optimized parameters are fed back into the MC simulation model to derive the final optimized values. The superior optimization efficiency of the HRG-MCO method is demonstrated through a comparative analysis with the exhaustive enumeration (EE) method and the standalone GA. To further validate its effectiveness, the method is applied to the optimization design of moderator-collimator for accelerator-based thermal neutron radiography. Two optimization tasks are performed in this study: (1) determining the optimal efficiencies under different source neutron energies and (2) optimization of thermal neutron-induced photon yield ratio. The results underscore the effectiveness and practical applicability of the HRG-MCO method in neutronics optimization design.

Full Text

Preamble

A new Monte Carlo optimization (MCO) method named Hybrid Adaptive Response Surface Methodology-Genetic Algorithm (RSM-GA) Monte Carlo Optimization (HRG-MCO) is proposed to address the strong empirical dependence

and low efficiency of global multi-parameter optimization in traditional neutronics design. HRG-MCO integrates the advantages of Response Surface Methodology (RSM) and Genetic Algorithm (GA). Specifically, neutron MC simulation results are iteratively utilized to adaptively construct an RSM model, ensuring the required accuracy. Subsequently, GA is employed to perform multi-parameter optimization based on the constructed RSM model, which makes it possible to rapidly determine the optimal design parameters. These optimized parameters are then fed back into the MC simulation model to derive the final optimized values. The superior optimization efficiency of the HRG-MCO method is demonstrated through a comparative analysis with the exhaustive enumeration (EE) method and the standalone GA. To further validate its effectiveness, the method is applied to the optimization design of moderator-collimator for accelerator-based thermal neutron radiography. Two optimization tasks are performed in this study: (1) determining the optimal efficiencies under different source neutron energies and (2) optimization of thermal neutron-induced photon yield ratio. The results underscore the effectiveness and practical applicability of the HRG-MCO method in neutronics optimization design.

Keywords: Neutronics Optimization Design, Monte Carlo Optimization (MCO), Response Surface Methodology (RSM), Genetic Algorithm (GA), Thermal Neutron Radiography

INTRODUCTION

In recent years, neutron-based nuclear technologies—such as advanced nuclear energy systems, boron neutron capture therapy (BNCT), and neutron radiography—have undergone rapid development [**?**, **?**, **?**, **?**, **?**]. The Monte Carlo Optimization (MCO) method is widely used in neutron system design due to its intuitive modeling and high computational accuracy [**?**, **?**, **?**, **?**, **?**, **?**, **?**, **?**]. However, traditional MCO methods, which rely on exhaustive enumeration (EE) method or gradient-based approaches, require significant expertise from designers and struggle to balance multiple design factors and objectives, leading to optimization results that lack systematic and global efficiency [**?**, **?**].

Genetic Algorithm (GA), with its powerful multi-parameter optimization capabilities, has been widely applied in MCO in recent years. For example, in 2019, Byoungil Jeon et al. proposed an optimization method combining GA with MC simulations to simultaneously calculate energy calibration parameters and gamma response functions [**?**]. In the same year, Guang Hu et al. used GA to optimize the moderator structure based on the neutron energy spectrum output from MCNP5 [**?**]. In 2020, M.F. Yan et al. proposed an optimization method that integrates GA with MCNP for the design of fast neutron imaging collimators to enhance neutron intensity, uncollided fraction, and the n/ ratio [**?**]. In 2022, S. Bagheri applied an intelligent method based on GA, integrated with the MCNP program, to optimize the radiation shielding system of a small nuclear reactor, demonstrating higher optimization efficiency compared to traditional design methods [**?**]. In 2023, F. Cordella et al. combined GA with

MCNP6 and Geant4 for radiation shielding optimization [**?**]. Although GA offers higher optimization efficiency than EE, the inherent randomness in their crossover and mutation processes can lead to a significant number of redundant computations. As a result, in large-scale, high-precision optimization problems or those involving variable boundary conditions, GA still becomes impractical due to the high computational cost of MC simulations.

Response Surface Methodology (RSM), on the other hand, optimizes by constructing multi-parameter function surface models and is currently another well-established multi-parameter optimization method. Due to the fast computational speed of function models, RSM offers high optimization efficiency. However, the accuracy of the RSM model construction directly impacts the final optimization results [**?**, **?**, **?**, **?**, **?**]. Therefore, building a high-accuracy RSM analysis model is key to the successful application of RSM.

This study presents a novel hybrid methodology that synergistically integrates RSM and GA to enhance neutronic design optimization efficiency. As a proof of concept, we apply this approach to optimize the moderator-collimator configuration for accelerator-based thermal neutron radiography systems, effectively addressing concurrent optimization challenges including moderation efficiency under different source neutron energies and thermal neutron-induced photon yield ratio.

II. RESEARCH METHODS

A. Theory for the Method

1. Monte Carlo Simulation Method The MC method is a computational technique based on probability and statistics, which leverages computer simulations of stochastic processes to obtain approximate solutions [**?**, **?**]. The primary MC simulation software with neutron transport capabilities includes MCNP [**?**], OpenMC [**?**], and Geant4 [**?**]. In this study, the Geant4 software package is employed. Developed by CERN using C++ object-oriented technology, Geant4 is a large-scale open-source software package capable of simulating the physical transport processes of various particles, including neutrons, in matter. Due to its versatility and scalability, Geant4 has been widely applied across various fields, including nuclear technology applications. To further improve the computational efficiency of neutron transport, this study also employs the Gamos extension package compatible with Geant4 to achieve geometry importance sampling acceleration [**?**].

2. Latin Hypercube Sampling Latin Hypercube Sampling (LHS) adopts a stratified sampling strategy that ensures each variable is uniformly distributed within its defined domain. The core idea is to divide the range of each variable into multiple equally spaced intervals and then randomly select one sample point from each interval, while avoiding overlap in lower-dimensional projections. This effectively reduces correlations between variables and enhances the

overall space-filling quality of the samples [**?**]. This means that regardless of the dimensionality, LHS can ensure a uniform distribution of sampling points across the space.

Although LHS has advantages in ensuring uniform distribution across each dimension, it may still fail to fully capture the true characteristics of the sampling space in certain scenarios. To overcome this limitation, several optimization criteria have been proposed, including the maximin and minimax distance criteria [**?**]. The maximin criterion aims to maximize the minimum distance between sample points, promoting dispersion, while the minimax criterion seeks to minimize the maximum distance between any point and its neighbors. In this study, the maximin criterion was adopted to ensure uniform distribution of sample points across the design space, thereby improving space-filling and coverage. This is particularly important for thoroughly exploring the design space and minimizing uncovered regions, ultimately enhancing the accuracy and reliability of the optimization results.

3. Response Surface Methodology RSM is a method that employs systematic experimental design to obtain data and uses a multivariate quadratic regression equation to model the functional relationship between influencing factors and response values [**?**]. The analysis of the regression equation facilitates the identification of optimal parameter combinations, thereby providing an effective means for addressing multivariate optimization problems.

The multivariate quadratic regression equation is expressed as:

$$y = \beta_0 + \sum \beta_i x_i + \sum \beta_{ii} x_i^2 + \sum \sum \beta_{ij} x_i x_j + \varepsilon \tag{1}$$

where y represents the predicted response value; β_0 denotes the regression intercept; β_i, β_{ii}, and β_{ij} correspond to the coefficients of linear, quadratic, and interaction terms, respectively; x_i and x_j are coded values of process variables; and ε accounts for residuals and experimental errors.

The traditional RSM typically employs second-order polynomials for response surface modeling, while higher-order polynomials are also widely used as fitting functions in RSM. It has been demonstrated that higher-order polynomials can effectively approximate various surface shapes within limited regions [**?**]. However, higher-order models tend to exhibit unstable behavior in unexplored regions of the design space and inherently demand greater computational resources to improve prediction accuracy [**?**]. Since higher-order polynomials involve more unknown coefficients and result in more complex functions, the selection of the polynomial order should be carefully considered.

In this study, given the requirements for optimized moderator-collimator system parameters and the semi-automated nature of the RSM process, the computational cost associated with implementing higher-order polynomials becomes negligible compared to the substantial resources required for MC simulations.

Therefore, higher-order polynomial models with different orders are self-adopted for response surface analysis to achieve the target accuracy in system optimization.

4. Genetic Algorithm GA is an optimization algorithm designed for searching optimal solutions, characterized by its ability to directly manipulate structural objects, operate without relying on derivatives or function continuity constraints, and exhibit implicit parallelism and global optimization capabilities. It adaptively adjusts search directions through probabilistic methods [**?**, **?**, **?**]. By simulating natural selection and genetic mutation processes, GA intelligently explores solutions to complex problems. The algorithm maintains a diverse population and iteratively improves solution quality through operations such as selection, crossover, and mutation, enabling effective exploration of potential optimal regions in the solution space without requiring gradient information from the objective function [**?**, **?**].

As an efficient multi-parameter optimization technique, GA has demonstrated significant computational load reduction in MCO applications. Figure 1 schematically illustrates the standard workflow for GA-based MCO [**?**].

[FIGURE:1]

In this study, GA-Based MCO is used to compare with the HRG-MCO to demonstrate the performance of the new method.

B. Establishment of HRG-MCO

The proposed method, named Hybrid Adaptive RSM-GA Monte Carlo Optimization (HRG-MCO), integrates RSM, MC, and GA using Python. The detailed optimization design workflow is illustrated in Figure 2.

First, HRG-MCO sets the preset accuracy of the RSM model. Then, based on the formulated optimization problem, the objective function and optimization variables for the GA are defined. LHS is used to select the initial trial points of the multidimensional design parameters to be optimized. These points are subsequently input into the MC model to calculate the neutron beam target parameters under different conditions. Unlike conventional GA-Based MCO, this approach does not directly use the MC-computed values for GA iteration. Instead, the calculated objective values are used to construct an adaptive RSM model. Since the fitting process of the RSM model is significantly faster than the MC computation of validation points, the adaptive modeling process fits eight RSM models from the third to the tenth order. LHS is also used to generate model validation points, which are then evaluated via MC simulations. Once the MC validation results are obtained, all models are validated for accuracy using Equation 2:

$$E = \frac{|y_1 - y_2|}{y_2} \times 100\% \tag{2}$$

Here, y_1 represents the predicted value, y_2 denotes the simulated value, and E represents the relative error between the two. After evaluating the accuracy of all fitted models, their performance is compared against a predefined accuracy threshold to determine whether the required accuracy has been achieved. If none of the models meet the accuracy criteria, the validation data from the current iteration are incorporated into the model fitting process, and a new set of validation points is generated through resampling for the next round of accuracy assessment. This process is repeated until at least one model satisfies the accuracy requirement. If models of different orders meet the criteria in the same round, the one with the highest accuracy will be selected for the subsequent GA optimization. The GA then identifies the optimal set of design variables based on the selected model. Finally, an MC simulation is conducted using these optimized variables to obtain the final optimized target value. To enhance the clarity and interpretability of the figures, only the data obtained from the highest accuracy model and its two neighboring order models are presented.

As the dimensionality of the optimization problem increases, the computational cost of constructing high-accuracy models grows exponentially. Appropriately relaxing the model accuracy requirements can significantly accelerate the convergence to a solution. In this study, the model validation error thresholds are set according to the problem dimensionality: 1% for two-dimensional problems, 3% for three-dimensional problems, and 5% for four-dimensional problems.

[FIGURE:2]

C. Validation of HRG-MCO

To validate the effectiveness of HRG-MCO, a two-factor Monte Carlo model was developed based on the classical optimization problem of D-T neutron source moderation design. A schematic diagram of the model is presented in Figure 3. The model consists of two cylindrical layers: (1) a tungsten multiplier layer with a diameter of 40 cm, and (2) a polyethylene moderation layer of the same diameter. The optimization range for both layers is confined to 1-20 cm. The 14 MeV source neutrons are incident from the left along the central axis of the cylinders. A thermal neutron point detector is positioned 20 cm to the right of the moderator surface along the model central axis to record thermal neutrons below 0.5 eV produced by the moderation process. During the initial and model validation phases, the LHS sampling size was set to 10 sample points in each case. The stopping criterion for the response surface model accuracy was set as 1%. The objective of the GA optimization was to maximize the thermal neutron flux recorded by the point detector.

[FIGURE:3]

Figure 4 shows the iterative results of the RSM model accuracy, with the red dashed line representing the 1% validation threshold. After four iterations, the verification error of the fourth-order model reached 0.84%, which was the minimum among all orders, satisfying the algorithm' s criterion. Based on this

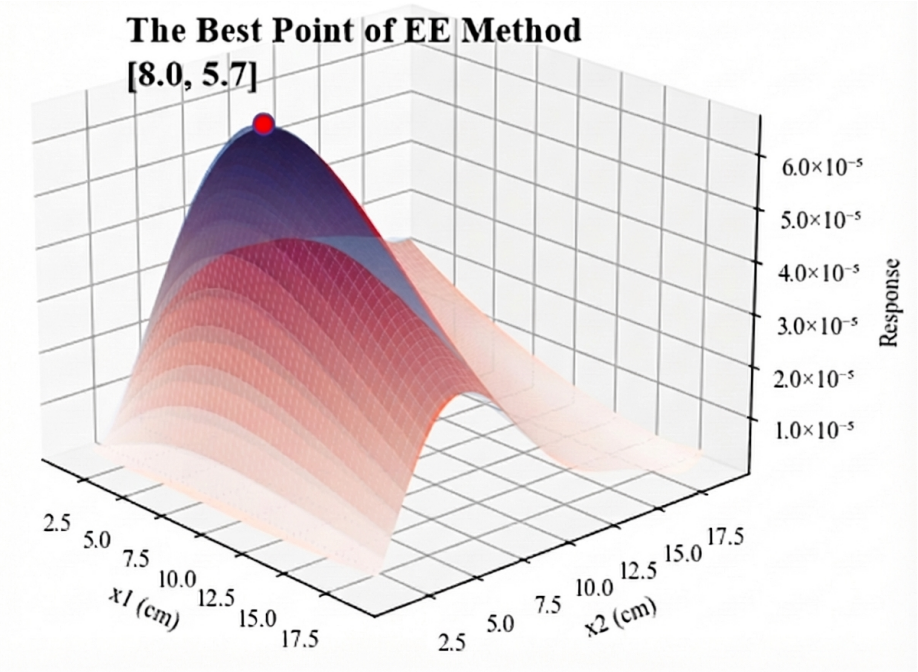

Figure 1: Figure 4

function model, the GA optimization was performed to determine the optimal parameters, which were identified as a neutron multiplier layer thickness of 8.0 cm and a moderation layer thickness of 5.7 cm. Under these parameter conditions, MC simulations yielded a moderation efficiency of 6.610×10^{-5} for the system.

To verify the efficiency of HRG-MCO and the accuracy of its optimization results, the outcomes from HRG-MCO were compared with those produced by EE and GA-based MCO. Here, the calculation in EE was performed using a thickness interval of 0.1 cm; the parameters used for GA were as follows: a population size of 10, a crossover probability of 0.5, and a mutation probability of 0.2. The comparative results are presented in Figure 5 and Table 1. Figure 5 illustrates the comparison between the response surface model established by HRG-MCO (red) and that constructed via EE (blue), where x_1 represents the multiplier layer thickness and x_2 represents the moderator layer thickness, showing good consistency between the two across various contour levels. Table 1 details that the model validation errors during HRG-MCO convergence were consistently below the manually set 1% accuracy threshold across all three trials, confirming its robust performance. Furthermore, under the same MC model cumulative computation count, the GA results deviate by 7.17% relative to EE, while the deviation is reduced to 0.50% under triple computation count. These results indicate that HRG-MCO not only achieves higher optimization efficiency compared to both EE and GA but also maintains a high degree of computational accuracy.

III. APPLICATION OF HRG-MCO IN THE OPTIMIZATION OF MODERATOR-COLLIMATOR DESIGN FOR COMPACT THERMAL NEUTRON RADIOGRAPHY SYSTEMS

A. Study on Moderation Efficiency Under Different Incident Neutron Energies

Compact thermal neutron radiography systems typically utilize accelerator-based neutron sources [**?**, **?**, **?**]. Depending on the specific neutron-producing reaction channels or the accelerator beam energy, the energy of the source neutrons can be adjusted as needed. Since the energy of source neutrons directly influences the thermalization efficiency of the moderator-collimator system, determining the optimal moderation efficiency performance across different neutron energies is essential for selecting both the neutron source and the accelerator beam energy in neutron radiography systems design. In traditional methods, obtaining the moderation efficiency curve requires designing and optimizing the moderator-collimator for each discrete energy point, which is a time-consuming process. This limitation significantly restricts the rapid generation of the moderation efficiency curve and further complicates the quantitative assessment of how different heavy metal multipliers affect its

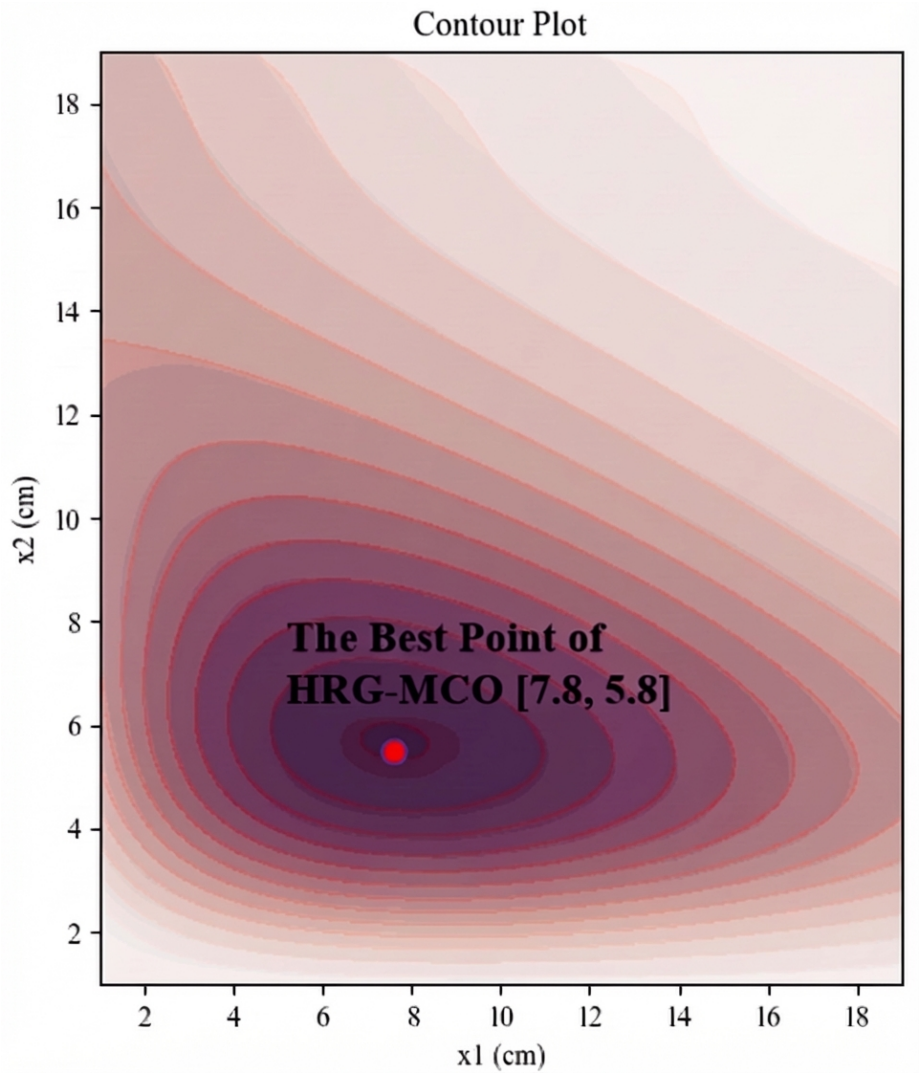

Figure 2: Figure 5

optimal configuration.

To address these issues, we conducted relevant research using HRG-MCO. First, an MC model of the moderator-collimator is established. Figure 6 shows a cross-sectional view along the central axis, where the yellow region represents the heavy metal multiplier layer, the green region represents the polyethylene moderator layer, and the blue region represents the graphite reflector. The inner wall of the collimation channel is lined with a Cd thermal neutron shielding layer, while the outermost layer of the moderator-collimator is a BC4 thermal shield. A 0.5 eV threshold thermal neutron point detector is placed at a collimation ratio (L/D) of 10. The detailed dimensions of the model are specifically marked in Figure 6. A mounting space for the accelerator target is reserved at the left entrance of the collimator. To simplify the model, the detailed structure of the accelerator target chamber was not included. Instead, a planar neutron source with a diameter of 20 mm was defined and placed perpendicular to the moderator-collimator axis on the left side of the multiplier layer. In the model, the parameters labeled 1 through 4 correspond to four optimization variables: (1) the thickness of the front-side neutron multiplier layer, (2) the thickness of the outer-side neutron multiplier layer, (3) the thickness of the polyethylene moderator layer, and (4) the energy of the source neutrons. Since the theoretical optimum for the reflector thickness is infinite, practical design constraints are taken into account. Accordingly, the radial graphite reflector thickness is set to 20 cm, and the axial graphite reflector thickness is set to 39 cm.

[FIGURE:6]

For the optimization design calculation, both the initial LHS sampling and the verification sampling were performed with a sample size of 100 points, and the RSM model verification accuracy was set to 5%. Figure 7 shows the final iterative calculation results for the RSM modeling verification accuracy, in which W was used as the neutron multiplying material. It can be observed that after multiple iterations, the verification accuracy of the eighth-order polynomial fit reached 4.96%, thereby achieving the targeted accuracy.

[FIGURE:7]

To obtain the optimal neutron moderating efficiency curve as a function of energy, energy values ranging from 1 to 14 MeV were sequentially input into the established RSM model at 0.5 MeV intervals. The output of the RSM model at each energy point was then used as the fitness function in the GA optimization process. The GA settings were as follows: a population size of 100, a crossover probability of 0.5, a mutation probability of 0.2, and 50 iterations. Figure 8 presents the dependence of optimized structural thicknesses on source neutron energy (a), and the variation of optimal moderation efficiency with respect to source neutron energy (b). A comparison of the data trends in the two figures indicates that the outer-side neutron multiplier layer becomes effective at relatively lower source neutron energies than the front-side layer. However, it primarily serves to slow the decline in moderation efficiency. In contrast, the

front-side neutron multiplier layer becomes active only at energies above 6 MeV, but it has a pronounced impact on enhancing the moderation efficiency.

Further analysis of Figure 8(b) reveals that the optimal moderation efficiency first decreases and then increases with rising incident neutron energy in the 1-14 MeV range, forming a broad V-shaped trend. This behavior can be attributed to the dominant moderation mechanisms at different energy levels. In the low to intermediate energy region, neutrons are primarily moderated via inelastic scattering. As the incident energy increases, more collisions are required for effective moderation, resulting in a gradual decline in moderation efficiency. However, when the incident energy exceeds the multiplication threshold of the material, a substantial number of secondary neutrons are generated through multiplication reactions. These secondary neutrons are then moderated, leading to a recovery in overall moderation efficiency.

To comparatively investigate the performance differences among multiplier layer materials including W, Pb, and depleted uranium (DU), the optimal moderation efficiency curves of Pb and DU were calculated using the same methodology described earlier. The comparative results are presented in Figure 9. The optimized parameters of each material layer are compared in Figure 10. As clearly demonstrated in Figure 9, a similar V-shaped trend is observed in three curves. However, DU consistently outperforms Pb and W in terms of overall efficiency. Figures 10(a) and 10(b) further indicate that the DU multiplier layer achieves this pronounced enhancement even with a relatively small thickness. To explain these observations, the neutron cross-sections of the three materials were obtained from the ENDF database and are presented in Figure 11. As shown in the figure, DU uniquely features a fission reaction channel, which enables the release of additional neutrons through fission, thereby significantly improving moderation efficiency. In addition, DU has a lower (n,2n) reaction threshold—approximately 6 MeV—compared to Pb and W, whose thresholds exceed 7 MeV (about 7 MeV for Pb and 7.5 MeV for W), making it more effective at lower incident neutron energies.

Further comparison of Figures 10(a) and 10(b), and Figure 11 reveals that the front-side multiplier layer tends to appear only after the (n,2n) reaction threshold is reached, whereas the lateral multiplier layer is present even at incident neutron energies below this threshold for all three materials. This can be attributed to the relatively high elastic scattering cross-sections of heavy metals, which enable them to reflect high-energy leakage neutrons back into the moderator region even before the onset of (n,2n) reactions. Such reflection enhances neutron utilization and contributes to improved moderation efficiency.

[FIGURE:8]

[FIGURE:9]

[FIGURE:10]

[FIGURE:11]

B. Optimization of Thermal Neutron-Induced Photon Yield Ratio

The combination of a neutron conversion screen and an optical imaging system is the most widely adopted imaging scheme in thermal neutron radiography systems [**?**, **?**, **?**]. In accelerator-based neutron sources, the source neutrons typically possess high energies. As a result, imaging quality is influenced not only by the thermal neutron flux but also degraded by the leakage of high-energy neutrons. This is primarily because high-energy neutrons are not constrained by the collimator channels and therefore do not exhibit the parallel-beam characteristics as thermal neutrons. Consequently, maximizing the ratio of thermal neutron-induced photon yield in the conversion screen becomes another key optimization objective in the design of the moderator-collimator for accelerator-based thermal neutron radiography. However, an inherent trade-off exists between thermal neutron flux and the photon yield ratio: improving the thermal neutron-induced photon yield ratio requires adding high-energy neutron-absorbing materials, but excessive use of these materials can reduce the transport efficiency of thermal neutrons.

Using the HRG-MCO method, this study investigates the optimization of the thermal neutron-induced photon yield ratio based on the same model shown in Figure 6, except that the source neutron energy is fixed at 14.1 MeV, corresponding to a D-T neutron source. W was selected as the metallic neutron multiplier layer due to its balanced performance characteristics and commercial availability.

Figure 12(a) shows the variation in photon yield of the 6LiF/ZnS thermal neutron conversion screen with incident neutron energy, which was obtained in previous research [**?**]. By convolving this curve with the neutron energy spectrum obtained from MC simulations of the moderator, the overall photon yield induced by the entire neutron field can be quantitatively assessed. As a preliminary study, to enhance computational efficiency, neutron energy is categorized into four energy regions: the thermal neutron region, epithermal neutron region, resonance neutron region, and fast neutron region, which are delineated in Figure 12(a) with red vertical dashed lines. The decision variables are consistent with the first three variables described in Section III.A. Figure 12(b) illustrates the high-order RSM validation results, where the sixth-order model first achieves the 3% accuracy target (red dashed line) after three iterations.

[FIGURE:12]

To optimize the thermal neutron-induced photon yield ratio, a GA objective function is constructed as defined in Equation 3:

$$\max F(x_1, x_2, x_3) = w_1 F_1 + w_2 F_2 + w_3 F_3 + w_4 F_4 \tag{3}$$

Here, F_5 represents the function that describes the thermal neutron-induced photon yield ratio relative to the total photon yield. The coefficients w_1 to w_4 correspond to the photon yield weights of thermal neutrons, epithermal

neutrons, resonance neutrons, and fast neutrons, as derived from Figure 12(a) and detailed in Table 2. F_1 to F_4 represent the neutron flux rates in the four energy regions, calculated based on the established RSM functions.

Based on Equation 3, the following NSGA-II optimization constraint functions can be further established, as expressed in Equation 4:

$$\max \begin{cases} \max F_1(x_1, x_2, x_3) \\ \max F_5(F_1, F_2, F_3, F_4) \end{cases} \tag{4}$$

subject to:

$$\begin{aligned} 0 < x_1 \leq 20 \\ 0 < x_2 \leq 20 \\ 0 < x_3 \leq 20 \end{aligned}$$

Here, F represents the overall objective function, x_1 to x_3, which represent three thicknesses to be optimized, were constrained to the range of 0 to 20 cm. The parameters for the NSGA-II are set as follows: The initial population size is 100, the parent population size (μ) is 100, the offspring population size (λ) is 200, the crossover probability is 0.5, the mutation probability is 0.2, and the maximum number of generations is 100. A blended crossover operator is employed, and Gaussian mutation is applied to balance solution diversity and convergence.

Figure 13 presents the Pareto front solutions from GA optimization, revealing a nonlinear inverse relationship between thermal neutron flux and thermal neutron-induced photon yield ratio. As the thermal neutron flux increases, the ratio decreases gradually. Analyzing the variation in the slope of the relationship curve indicates that when the thermal neutron-induced photon yield ratio is below 90%, the decline in thermal neutron flux is relatively moderate. However, once the ratio exceeds 90%, the thermal neutron flux begins to drop at a significantly accelerated rate.

[FIGURE:13]

The model parameters corresponding to the thermal neutron-induced photon yield ratio of 90% ($x_1 = 3.8$ cm, $x_2 = 5.6$ cm, $x_3 = 19.4$ cm) were incorporated into the MC model to recalculate the corresponding neutron energy spectrum, as shown in Figure 14(a). Based on this spectrum, the distribution of the thermal neutron-induced photon yield ratio as a function of neutron energy was further computed (Figure 14(b)). The results reveal that non-thermal neutrons dominate the total neutron flux, accounting for 91.8%. However, their contribution to the overall photon yield is only 9.9%. In contrast, thermal neutrons represent merely 8.2% of the total flux but are responsible for 90.1% of the overall photon yield.

[FIGURE:14]

IV. CONCLUSION

A novel method, Hybrid Adaptive RSM-GA Monte Carlo Optimization (HRG-MCO), is proposed and applied to the design of a moderator-collimator system for accelerator-based thermal neutron radiography. The key findings are summarized as follows:

1. Compared to EE and GA-based MCO approaches, HRG-MCO achieves high optimization accuracy (error $< 1\%$) using only about 50 sample points, demonstrating notable efficiency and robustness.
2. The optimal moderation efficiency curve across incident neutron energies (1-14 MeV) exhibits a V-shaped trend. Among the evaluated materials, depleted uranium (DU) shows the best performance due to its superior neutron multiplication characteristics.
3. In optimizing the photon yield for D-T neutron source-based radiography, a nonlinear trade-off is observed between thermal neutron flux and thermal neutron-induced photon yield ratio. Maintaining a 90% yield ratio allows retention of approximately 85% of the maximum thermal neutron flux.

While HRG-MCO demonstrates excellent efficiency and applicability, several limitations remain:

1. The current Latin Hypercube Sampling (LHS) provides uniform distribution across the design space but lacks targeted sampling in high-response regions. Introducing adaptive sampling strategies could improve convergence by focusing sample density where model sensitivity is highest.
2. Due to the stochastic nature of GA and the complexity of high-dimensional nonlinear problems, the optimization process may occasionally converge to local optima. Enhancing mutation strategies or combining GA with adaptive sampling techniques could further improve global search performance.
3. The polynomial-based RSM used in this study may struggle to capture intricate or localized nonlinear behavior, particularly in sparsely sampled regions. Future studies could explore more advanced surrogate models or hybrid fitting techniques to improve prediction accuracy and stability.

In conclusion, HRG-MCO proves to be a highly efficient and generalizable Monte Carlo-based optimization framework. Beyond thermal neutron radiography, it holds significant potential for broader applications, such as reactor shielding design, beam shaping assembly (BSA) optimization in BNCT systems, and particle transport modeling in radiation detection and protection technologies.

REFERENCES

[1] Y.N. Zhu, Z.K. Lin, H.Y. Yu et al., Study on the optimal incident proton energy of 7Li(p, n)7Be neutron source for boron neutron capture therapy. Nucl.

Sci. Tech. 35, 60 (2024). https://doi.org/10.1007/s41365-024-01420-6

[2] Y. Zhang, C. Liu, S.L. Liu et al., Prompt fission neutron uranium logging (II): dead-time effect of the neutron time spectrum. Nucl. Sci. Tech. 36, 19 (2025). https://doi.org/10.1007/s41365-024-01615-x

[3] Z.P. Qiao, Y.C. Hu, Q.X. Jiang et al., Coin-structured tunable beam shaping assembly design for accelerator-based boron neutron capture therapy for tumors at different depths and sizes. Nucl. Sci. Tech. 34, 186 (2023). https://doi.org/10.1007/s41365-023-01325-w

[4] Y. Kiyanagi, Neutron applications developing at compact accelerator-driven neutron sources. AAPPS Bull. 31, 22 (2021). https://doi.org/10.1007/s43673-021-00022-3

[5] Y. Sun, Q.B. Wang, P.C. Li et al., Indirect neutron radiography experiment on dummy nuclear fuel rods for pressurized water reactors at CMRR. Nucl. Sci. Tech. 35, 189 (2024). https://doi.org/10.1007/s41365-024-01534-x

[6] W.K. Chen, L.Q. Hu, G.Q. Zhong et al., Optimization study and design of scintillating fiber detector for D-T neutron measurements on EAST with Geant4. Nucl. Sci. Tech. 33, 139 (2022). https://doi.org/10.1007/s41365-022-01123-w

[7] X. Bai, J. Ma, Z. Wei et al., Development of a high-yield compact DD neutron generator. Nucl. Instrum. Meth. A 1069, 169993 (2024). https://doi.org/10.1016/j.nima.2024.169993

[8] C. Li, S. Jing, Y. Gao et al., MCNP optimization of fast neutron beam thermalization device based on D-T neutron generator. Fusion Eng. Des. 151, 111385 (2020). https://doi.org/10.1016/j.fusengdes.2019.111385

[9] W. Tang, J.G. Liang, Y. Ge et al., A method for neutron-induced gamma spectra decomposition analysis based on Geant4 simulation. Nucl. Sci. Tech. 33, 154 (2022). https://doi.org/10.1007/s41365-022-01144-5

[10] X.Y. Wang, J.Y. Chen, Q. Zhang, Boron shielding design for neutron and gamma detectors of a pulsed neutron tool. Nucl. Sci. Tech. 36, 16 (2025). https://doi.org/10.1007/s41365-024-01605-z

[11] D. Prastowo, Design of neutron activation and radiography facilities based on DD generator. Indones. J. Phys. 34, 1-7 (2023). https://doi.org/10.5614/itb.ijp.2023.34.2.1

[12] J.L. Wang, L.A. Cruz, Q.B. Wu et al., Radiation shielding design of a compact single-room proton therapy based on synchrotron. Nucl. Sci. Tech. 31, 1 (2020). https://doi.org/10.1007/s41365-019-0712-1

[13] Z.L. Zhao, Y.W. Yang, S. Hong, Application of FLUKA and OpenMC in coupled physics calculation of target and sub-critical reactor for ADS. Nucl. Sci. Tech. 30, 10 (2019). https://doi.org/10.1007/s41365-018-0539-1

[14] H.Y. Li, C.Y. Zhao, S. Qiao et al., Design of moderator and collimator systems for compact neutron radiography. Nucl. Instrum. Meth. A 959, 163535 (2020). https://doi.org/10.1016/j.nima.2020.163535

[15] D. Prastowo, Design of Neutron Activation and Radiography Facilities Based on DD Generator. Indones. J. Phys. 34(2), 1-7 (2023). https://doi.org/10.5614/itb.ijp.2023.34.2.1

[16] B. Jeon, J. Kim, M. Moon et al., Parametric optimization for energy calibration and gamma response function of plastic scintillation detectors using a genetic algorithm. Nucl. Instrum. Meth. A 930, 8-14 (2019). https://doi.org/10.1016/j.nima.2019.03.003

[17] G. Hu, Y.Y. Ren, R.R. Cui et al., A novel method for designing the moderator of accelerator-driven neutron source. Ann. Nucl. Energy 133, 96-99 (2019). https://doi.org/10.1016/j.anucene.2019.04.056

[18] M.F. Yan, G. Hu, B. Liu et al., Optimization design of a fast neutron imaging collimator by genetic algorithm. J. Instrum. 15(12), P12002 (2020). https://doi.org/10.1088/1748-0221/15/12/P12002

[19] S. Bagheri, H. Khalafi, SMR, 3D exact source term simulation for shielding design based on genetic algorithm. Ann. Nucl. Energy 191, 109915 (2023). https://doi.org/10.1016/j.anucene.2023.109915

[20] F. Cordella, M. Cappelli, M. Ciotti et al., Genetic algorithm for multilayer shield optimization with a custom parallel computing architecture. Eur. Phys. J. Plus 139, 150 (2024). https://doi.org/10.1140/epjp/s13360-023-04842-0

[21] S. Çam Kaynar, Ü.H. Kaynar, Method for the determination of polonium-210 in tea samples using response surface methodology (RSM). Nucl. Sci. Tech. 30, 45 (2019). https://doi.org/10.1007/s41365-019-0567-5

[22] Y.C. Gao, L.Z. Cao, W.L. Ye et al., Neutronics design optimization of a small modular fast reactor based on response surface methodology. Nucl. Eng. Des. 395, 111860 (2022). https://doi.org/10.1016/j.nucengdes.2022.111860

[23] S.M. Baligidad, U. Chandrasekhar, K. Elangovan et al., RSM optimization of parameters influencing mechanical properties in selective inhibition sintering. Mater. Today Proc. 5(2), 4903-4910 (2018). https://doi.org/10.1016/j.matpr.2017.12.067

[24] A. Ahmad, A.K. Yadav, A. Singh, Process optimization of spirulina microalgae biodiesel synthesis using RSM coupled GA technique: a performance study of a biogas-powered dual-fuel engine. Int. J. Environ. Sci. Technol. 21(1), 169-188 (2024). https://doi.org/10.1007/s13762-023-04948-z

[25] G. Rahimi, D. Chirlesan, Z. Soltani, Optimization of filler content and minimizing thickness of polymeric composite for shielding against neutron source by Response Surface Methodology (RSM) and Monte Carlo simulation. Eur. Phys.

J. Spec. Top. 232(10), 1657-1663 (2023). https://doi.org/10.1140/epjs/s11734-023-00904-7

[26] I. Lux, Monte Carlo Particle Transport Methods, 1st edn. (CRC Press, 1991). https://doi.org/10.1201/9781351074834

[27] Z.P. Chen, A.K. Sun, J.C. Lei et al., Multi-function and generalized intelligent code-bench based on Monte Carlo method (MagicMC) for nuclear applications. Nucl. Sci. Tech. 36, 57 (2025). https://doi.org/10.1007/s41365-024-01626-8

[28] Los Alamos National Lab. (LANL), MCNP: a general Monte Carlo code for neutron and photon transport. Tech. Rep., Nov. 1979. https://doi.org/10.2172/5823239

[29] P.K. Romano, N.E. Horelik, B.R. Herman et al., OpenMC: A state-of-the-art Monte Carlo code for research and development. Ann. Nucl. Energy 82, 90-97 (2015). https://doi.org/10.1016/j.anucene.2014.07.048

[30] S. Agostinelli, J. Allison, K. Amako et al., GEANT4—a simulation toolkit. Nucl. Instrum. Meth. A 506(3), 250-303 (2003). https://doi.org/10.1016/S0168-9002(03)01368-8

[31] P. Arce, F. Sansaloni, J. Lagares, Point Detector Scorer in GAMOS/Geant4. IEEE Nucl. Sci. Symp. Med. Imaging Conf., Knoxville, TN, USA, 2010, pp. 1182-1184. https://doi.org/10.1109/NSSMIC.2010.5873954

[32] P. Borisut, A. Nuchitprasittichai, Adaptive Latin Hypercube Sampling for a Surrogate-Based Optimization with Artificial Neural Network. Processes 11(11), 3232 (2023). https://doi.org/10.3390/pr11113232

[33] M.E. Johnson, L.M. Moore, D. Ylvisaker, Minimax and maximin distance designs. J. Stat. Plan. Inference 26(2), 131-148 (1990). https://doi.org/10.1016/0378-3758(90)90122-B

[34] D.C. Montgomery, Design and Analysis of Experiments (Wiley, 2017). https://doi.org/10.1007/978-3-319-52250-0

[35] K. Al-Ghamdi, E. Aspinwall, Modelling an EDM Process Using Multilayer Perceptron Network, RSM, and High-Order Polynomial. Adv. Mech. Eng. 2014, 1-16 (2014). https://doi.org/10.1155/2014/791242

[36] M.R. Rajashekhar, A new look at the response surface approach for reliability analysis. Struct. Saf. 12(3), 205-220 (1993). https://doi.org/10.1016/0167-4730(93)90003-J

[37] Z. Michalewicz, C.Z. Janikow, GENOCOP: a genetic algorithm for numerical optimization problems with linear constraints. Commun. ACM 39(12), 175 (1996). https://doi.org/10.1145/272682.272711

[38] O. Castillo, P. Melin, Genetic Algorithms and Simulated Annealing. In: Soft Computing for Control of Non-Linear Dynamical Systems. Stud. Fuzziness

Soft Comput. 63 (Physica, Heidelberg, 2001). https://doi.org/10.1007/978-3-7908-1832-0

[39] S. Mirjalili, Genetic Algorithm. In: Evolutionary Algorithms and Neural Networks. Stud. Comput. Intell. 780 (Springer, Cham, 2019). https://doi.org/10.1007/978-3-319-93025-1_4

[40] C.X. Gu, M.Q. Wu, G. Lin, et al., The global optimization design for electron emission system using genetic algorithms. Nucl. Instrum. Meth. A 519(1-2), 90-95 (2004). https://doi.org/10.1016/j.nima.2003.11.126

[41] Z.Y. Dai, Y.C. Nie, Z. Hui, et al., Design of S-band photoinjector with high bunch charge and low emittance based on multi-objective genetic algorithm. Nucl. Sci. Tech. 34, 41 (2023). https://doi.org/10.1007/s41365-023-01183-6

[42] H.Y. Li, C.Y. Zhao, S. Qiao, et al., Design of moderator and collimator systems for compact neutron radiography. Nucl. Instrum. Meth. A 959, 163535 (2020). https://doi.org/10.1016/j.nima.2020.163535

[43] S. Wang, W. Yin, B. Liu, et al., A moveable neutron imaging facility using D-T neutron source based on a compact accelerator. Appl. Radiat. Isot. 169, 109564 (2021). https://doi.org/10.1016/j.apradiso.2020.109564

[44] H.Y. Li, D.X. Zhang, C.Y. Zhao, et al., Improvement of moderation efficiency for neutron source system in compact neutron radiography device. Nucl. Instrum. Meth. A 1015, 165760 (2021). https://doi.org/10.1016/j.nima.2021.165760

[45] W. Chuirazzi, A. Craft, B. Schillinger, et al., Performance testing of dysprosium-based scintillation screens and demonstration of digital transfer method neutron radiography of highly radioactive samples. Nucl. Technol. 208(3), 455-467 (2021). https://doi.org/10.1080/00295450.2021.1905471

[46] B. Schillinger, W. Chuirazzi, A. Craft, et al., Performance of borated scintillator screens for high-resolution neutron imaging. J. Radioanal. Nucl. Chem. 331, 5287-5295 (2022). https://doi.org/10.1007/s10967-022-08477-w

[47] S.R. Miller, M.S.J. Marshall, M. Wart, et al., High-resolution thermal neutron imaging with 10Boron/CsI:Tl scintillator screen. IEEE Trans. Nucl. Sci. 67(8), 1929-1933 (2020). https://doi.org/10.1109/TNS.2020.3006741

[48] L.X. Zhang, S.Z. Chen, Z.D. Zhang, et al., Resolution analysis of thermal neutron radiography based on accelerator-driven compact neutron source. Nucl. Sci. Tech. 34, 76 (2023). https://doi.org/10.1007/s41365-023-01227-x